Int. J. Heat Mass Transfer. Vol. 35, No. 10, pp. 2593–2604, 1992
Printed in Great Britain

0017–9310/92 $5.00 + 0.00

Influence of high mainstream turbulence on leading edge film cooling heat transfer: effect of film hole spacing

A. B. MEHENDALE and J. C. HAN

Turbine Heat Transfer Laboratory, Mechanical Engineering Department, Texas A&M University, College Station, TX 77843, U.S.A.

(*Received* 22 *July* 1991 *and in final form* 17 *September* 1991)

Abstract—The effect of injection hole geometry on the leading edge heat transfer coefficient and film cooling effectiveness, under high mainstream turbulence condition, was experimentally studied for an incident mainstream Reynolds number of 100 000. Data were obtained for three blowing ratios of 0.4, 0.8 and 1.2 through two rows of film holes located at ±15 and ±40° for two injection geometries: (a) film holes spaced four hole diameters apart and (b) film holes spaced three hole diameters apart, in the spanwise direction. The results show that the leading edge heat transfer coefficient increases and the film effectiveness decreases with increasing mainstream turbulence; however, the effect reduces with increasing blowing ratio. The leading edge heat transfer with coolant injection (heat load) for the three hole diameters case is lower than that for the four hole diameters case at low mainstream turbulence, but the difference reduces at higher mainstream turbulence.

INTRODUCTION

GAS TURBINES are frequently operated at high turbine inlet temperatures to achieve better performance and turbine component cooling is required to withstand such high temperatures. The film cooling technique has been extensively applied to gas turbine airfoils, around the leading edge and on both pressure and suction sides to reduce the airfoil surface temperature. The heat transfer coefficient and film effectiveness distributions over the entire airfoil depend on the mainstream flow condition and its interaction with the secondary injection flow condition (due to: number of rows of film holes, film hole row location from stagnation, spanwise spacing of film holes, film hole angle, and film hole shape, etc.). Therefore, it is essential to study the effect of secondary coolant injection conditions on the heat transfer coefficient and film effectiveness distributions.

A gas turbine airfoil without film cooling is shown in Fig. 1. The local convective heat flux (heat load) is given by

$$q_0'' = h_0(T_\infty - T_w), \tag{1}$$

where q_0'' is the local convective heat load without film cooling, h_0 is the local heat transfer coefficient without secondary injection, T_∞ is the hot mainstream gas temperature, and T_w is the local wall temperature.

The local heat transfer coefficient, h_0, is a function of only the flow conditions and can be evaluated separately. Knowing T_∞ and T_w, the local heat load can be evaluated from equation (1).

A gas turbine airfoil with film cooling is also shown in Fig. 1. The convective heat load at any location is given by

$$q'' = h(T_f - T_w), \tag{2}$$

where q'' is the local convective heat load with secondary injection, h is the local heat transfer coefficient with secondary injection, T_f is the local film temperature (local mixing temperature between mainstream and coolant), and T_w is the local wall temperature.

The local heat transfer coefficient with film cooling (h) is a function of only the flow conditions due to

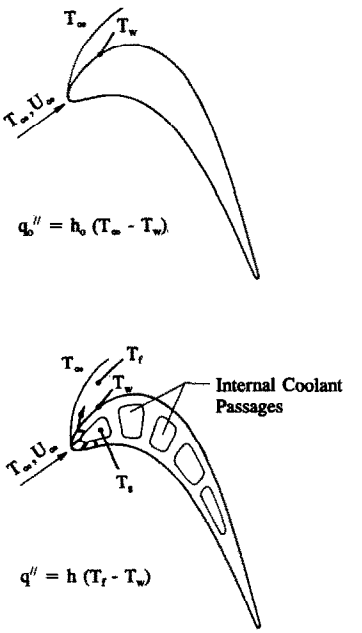

FIG. 1. Turbine airfoil without and with film cooling.

NOMENCLATURE

b	width of turbulence grid bars
B	blowing ratio (average secondary-to-mainstream mass flux ratio)
d	film hole diameter
D	leading edge diameter
h	local convective heat transfer coefficient with film cooling
h_0	local convective heat transfer coefficient without film cooling
k	fluid thermal conductivity
L	film hole length
L_e^u	dissipation length scale
$\dot{m}_{15}$	mass flow rate through film holes at $\pm 15°$
$\dot{m}_{40}$	mass flow rate through film holes at $\pm 40°$
n	number of thermocouples in a spanwise row at any streamwise location
Nu_D	local Nusselt number based on leading edge diameter D
$\overline{Nu}_D$	spanwise averaged Nusselt number
P	pitch of film holes in a row
q''	local convective heat flux with film cooling
$\bar{q}''$	spanwise averaged convective heat flux with film cooling
q''_{cond}	local conduction heat flux
q''_{gen}	local foil generated surface heat flux
q''_{rad}	local radiation heat flux
q''_0	local convective heat flux without film cooling
$\bar{q}''_0$	spanwise averaged convective heat flux without film cooling
Re_D	Reynolds number based on incident mainstream velocity U_∞ and leading edge diameter D
T_{aw}	local adiabatic wall temperature
T_f	local film temperature
T_s	secondary (injected) air temperature just before injection
T_w	local wall temperature
T_∞	mainstream air temperature
Tu	local streamwise turbulence intensity
U	local mainstream velocity
U_∞	incident mainstream velocity at $X/b = 20$ for no grid case
x	streamwise distance from stagnation (along test surface)
X	axial distance from turbulence grid location
z	spanwise distance.

Greek symbols

η	film effectiveness
$\bar{\eta}$	spanwise averaged film effectiveness
ϕ	overall cooling effectiveness.

secondary flow interaction with the mainstream and can be determined separately. The wall temperature T_w is also known; however, the film temperature T_f is an unknown that cannot be readily determined.

To solve this problem, a dimensionless film temperature (commonly known as film effectiveness) is defined as

$$\eta = \frac{T_\infty - T_f}{T_\infty - T_s} \tag{3}$$

where η is the local film cooling effectiveness, T_∞ is the hotter mainstream temperature, T_f is the intermediate local film temperature, and T_s is the cooler secondary flow temperature just before injection.

Local film effectiveness, η, is determined from laboratory models by making some assumptions and simplifications that will be discussed later. Since η is nondimensional, after substituting the appropriate values of T_∞ and T_s for actual gas turbine conditions, a corresponding value of T_f is obtained. The local heat load with secondary injection can be evaluated by substituting this value of T_f in equation (2).

Since the objective of film cooling is to reduce the surface heat transfer of an airfoil, heat loads with and without film cooling should be compared. From equations (1) and (2), the local heat load ratio is given by

$$\frac{q''}{q''_0} = \frac{h}{h_0}\frac{T_f - T_w}{T_\infty - T_w} \tag{4}$$

where a heat load ratio of less than unity indicates that film cooling causes a reduction in surface heat transfer over the no film cooling case.

The importance of studying local film effectiveness distributions has been explained previously. From equation (4), since $T_w < T_f < T_\infty$, the ratio of temperatures is less than unity. Owing to interaction of the secondary flow and mainstream, we expect higher heat transfer coefficients for the film cooled case over the no film cooling case, i.e. $h > h_0$. Hence, it is equally important to study the local heat transfer coefficient distributions for the no film cooling and with film cooling cases to see if this disadvantage (due to increased heat transfer coefficients) overrides the advantage due to a reduced source temperature (T_f instead of T_∞ in equation (4)).

There have been many investigations concerning film cooling of flat or mildly curved surfaces for various blowing ratios, injection geometries, and film coolants at low mainstream turbulence intensities (Goldstein [1], Eriksen and Goldstein [2], Mayle *et al.* [3], Ito *et al.* [4], and Han and Mehendale [5]).

Sasaki *et al.* [6] studied two row film cooling in the stagnation region of a circular cylinder in cross-flow.

Luckey and L'Ecuyer [7] studied the effect of a spanwise film hole angle for angles of 20, 30 and 40°. Luckey and L'Ecuyer [8] and Bonnice and L'Ecuyer [9] studied a circular cylinder with one to five rows of spanwise injection holes with various blowing ratios for low mainstream turbulence. Karni and Goldstein [10] used the naphthalene sublimation technique to study the effect of surface injection from a circular cylinder in cross-flow with one row of inclined holes on local mass transfer for low mainstream turbulence.

Mick and Mayle [11] used a blunt body with a circular leading edge and a flat afterbody to study in detail the film effectiveness and surface heat transfer coefficient for secondary air injection through two rows of inclined holes into the stagnation region of an incident mainstream flow for low mainstream turbulence intensity. Nirmalan and Hylton [12] studied the effects of exit Mach number, exit Reynolds number, coolant-to-gas temperature ratio, and coolant-to-gas pressure ratio on the turbine vane heat transfer coefficient with leading edge and downstream film cooling for low mainstream turbulence.

Mehendale and Han [13] studied the effect of high mainstream turbulence on leading edge film effectiveness and heat transfer coefficient for the case of flow over a test surface similar to Mick and Mayle [11]. Turbulence was generated by a turbulence grid (9.67%) and a jet-grid (12.9%) at a Reynolds number of 100 000. Film injection was through two rows of film holes at ± 15 and $\pm 40^{\circ}$ with blowing ratios of 0.4, 0.8 and 1.2.

Ou *et al.* [14] used the test model of Mehendale and Han [13] to study the effect of film hole row location on leading edge film cooling effectiveness and heat transfer under high mainstream turbulence levels ($Tu = 5.07$–12.9%). For a Reynolds number of 100 000 and blowing ratios of 0.4, 0.8 and 1.2, they investigated two cases of film injection: film holes located at $\pm 15^{\circ}$ from stagnation and film holes located at $\pm 40^{\circ}$ from stagnation.

This paper focuses on the effect of spanwise film hole spacing on leading edge film effectiveness and heat transfer coefficient under turbulence grid generated high mainstream turbulence conditions. Results for film holes spaced $4d$ apart are compared with the results published previously of Mehendale and Han [13] for film holes spaced $3d$ apart. High mainstream turbulence is produced by a turbulence grid ($Tu = 9.67\%$). The incident mainstream Reynolds number based on cylinder diameter is 100 000 for flow across a blunt body with a semi-cylinder leading edge and a flat afterbody. Spanwise and streamwise distributions of the local heat transfer coefficient and local film effectiveness are obtained from stagnation to the end of the flat afterbody. The objectives of this study are to (a) compare the effect of film hole spacing on film effectiveness and heat transfer coefficient downstream of the film holes and (b) determine which film hole geometry provides the lower heat load.

TEST APPARATUS AND INSTRUMENTATION

A schematic of the low speed, open circuit wind tunnel used is shown in Fig. 2. The test apparatus was designed as a suction type wind tunnel with a 7.5 kW (10 hp) blower. Upstream of the test section were a flow straightener and a flow nozzle for uniform oncoming flow conditions. The test duct was 25.4 cm × 76.2 cm and 183 cm long. Flow velocity was varied by controlling a sliding gate on the exhaust end of the blower. The mainstream temperature was maintained within $\pm 1^{\circ}$C of the desired value by a central air-conditioning unit. High mainstream turbulence was produced by a turbulence grid ($Tu = 9.67\%$) also shown in Fig. 2. The grid open area was 54%.

The test model was a blunt body with a semi-cylinder leading edge and a flat afterbody as shown in Fig. 3. The leading edge was 15.2 cm in diameter. This created a 20% flow blockage. The film holes were 1.1 cm in diameter and spaced $4d$ apart in the spanwise direction. Film injection rows were located at ± 15 and $\pm 40^{\circ}$ and were inclined at 30 and 90° to the test model surface in the spanwise and streamwise directions, respectively. The test model had one inlet port from below for the coolant. A secondary system supplied air for leading edge film cooling.

Strips of 0.05 mm thick stainless steel foil, each 25 cm long and 3.8 cm wide, were cemented vertically on the outer surface of the test model. They were separated from each other by 0.8 mm gaps. Holes were cut in the leading edge foils to match the film cooling holes in the test model. All foils were electrically connected in series by copper bus bars. The 0.8 mm gaps were filled and made flush with the foil surface by silicone caulk. The test surface acted as a constant heat flux test surface (except for the foils with film holes cut in them) when heated for heat transfer tests, otherwise, it acted as a near adiabatic surface for film cooling tests. Thermocouples in the bottom-most injection holes measured the film temperature just before injection.

Eighty-eight calibrated, 36 gage copper–constantan thermocouples were cemented on the underside of the foils; 73 were distributed in the leading edge region and 15 in the flat sidewall region. Additional thermocouples were attached on the inner wall of the test model to estimate conduction through the wood. All thermocouples were connected to a 100 channel Fluke 2280A datalogger interfaced with an IBM PC. A variac controlled the voltage across the stainless steel foils. Circuit voltage and current were measured by a Beckmann digital multimeter and an autoranging AWG current clamp, respectively.

A TSI IFA 100 constant temperature anemometer (CTA) together with a TSI IFA 200 high speed digitizer measured turbulence and velocity data from a calibrated single hot wire. The single component streamwise r.m.s. calculations were based on 1032 readings from the CTA. The local streamwise turbulence intensity was based on the average of five sets of r.m.s.

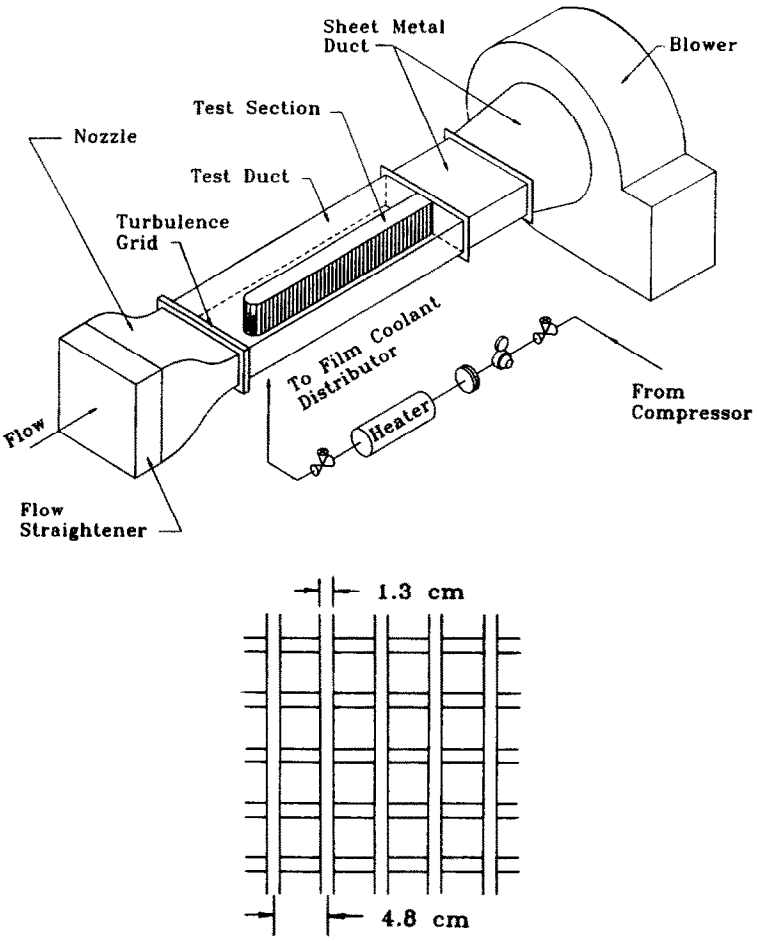

FIG. 2. Schematic of the film cooling test apparatus.

values (5160 readings) normalized by the local average streamwise velocity. The total digitizing time for the 5160 readings was about 0.5 s.

TEST CONDITIONS AND DATA ANALYSIS

Flow symmetry was confirmed by measuring the corresponding mainstream flow velocities on either side of the test model. Tests were conducted in the low turbulence wind tunnel for a Reynolds number of 100 000 based on a leading edge diameter D and incident mainstream velocity U_∞. Mainstream streamwise turbulence intensities for the no grid and turbulence grid cases were 0.75 and 9.67%, respectively. Nominal blowing ratios (based on the average secondary mass flux) of 0.4, 0.8 and 1.2 were used.

At the exit of each film hole in a row, the centerline velocity was within $\pm 5\%$ for $\pm 15^\circ$ rows and $\pm 4\%$ for $\pm 40^\circ$ rows. The secondary flow turbulence intensity (the r.m.s. fluctuations in the secondary flow at the exit of each hole, normalized by the incident mainstream velocity with mainstream flow on) was found to be 3–5%, 7–12% and 25–30% for blowing ratios of 0.4, 0.8, and 1.2, respectively. The turbulence intensity at the exit of film holes in any row was fairly uniform. The $\dot{m}_{40^\circ}/\dot{m}_{15^\circ}$ ratio was found to be 2.0, 1.5, and 1.2 for average blowing ratios of $B = 0.4$, 0.8, and 1.2, respectively.

As indicated in Mehendale *et al.* [15], heat transfer tests without film cooling were conducted for ambient mainstream flow and heated wall conditions. Hence, for data reduction purposes, equation (1) was modified to

$$h_0 = \frac{q_0''}{T_w - T_\infty} \tag{5}$$

where h_0 is the local heat transfer coefficient without film cooling, q_0'' is the local convective heat load without film cooling, T_w is the local heated wall temperature without film cooling, and T_∞ is the ambient mainstream temperature.

In the present study, for heat transfer tests, the secondary air temperature was almost the same as the mainstream (within $\pm 1^\circ$C); whereas, for film cooling

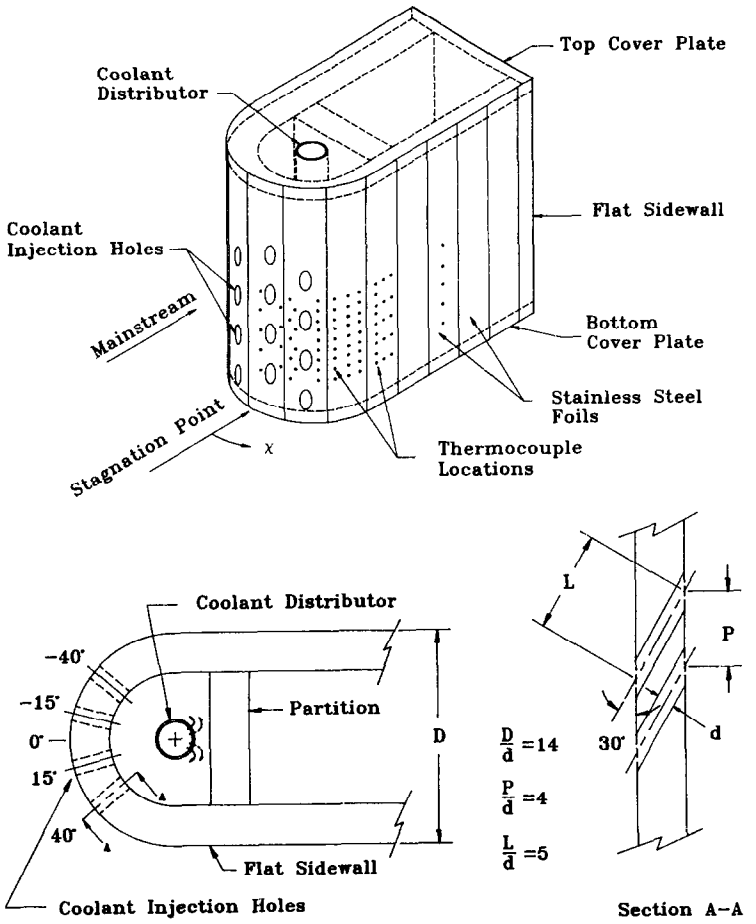

FIG. 3. Schematic of the leading edge with $4d$ hole spacing.

tests, the secondary air temperature was about 25°C higher than the mainstream. This resulted in a secondary-to-mainstream density ratio of 0.9. The density ratio is an important parameter. This study is for a constant density ratio condition.

Since heat transfer tests were conducted by injecting ambient air through the film holes into an ambient mainstream while power was being supplied to the surface foils, equation (2) was modified to

$$h = \frac{q''}{T_w - T_f} \tag{6}$$

where h is the local heat transfer coefficient with film cooling, q'' is the local convective heat load with film cooling, T_w is the local heated wall temperature, and T_f is the local cooler film temperature resulting from the mixing of ambient mainstream and ambient secondary flows.

Hence, T_f can be replaced by T_∞ and from equation (6)

$$h = \frac{q''}{T_w - T_\infty}. \tag{7}$$

Since the test model was not perfectly adiabatic, equation (7) was modified to

$$h = \frac{q''_{gen} - q''_{cond} - q''_{rad}}{T_w - T_\infty} \tag{8}$$

where h is the local heat transfer coefficient with film injection, q''_{gen} is the local generated surface heat flux, q''_{cond} is the local condution loss flux through the test model, q''_{rad} is the local radiation loss flux to the surroundings, T_w is the local wall temperature with power supply to foils for ambient mainstream and ambient secondary flows, and T_∞ is the ambient mainstream temperature.

For foils without film holes cut in them, there is no spanwise variation in q''_{gen} and it can be calculated easily. For foils with film holes cut in them, the generated surface heat flux varied considerably in the spanwise direction. A complete discussion about estimating this non-uniform flux is given in Mehendale and Han [13]. Loss tests were performed on the two test models to estimate the conduction loss. The conduction and the radiation heat losses were about 3 and 10%, respectively, of the generated heat. Heat loss through thermocouple wires was estimated to be very small (less than 0.1%); axial and lateral conduction through the thin foil was also found to be negligible (less than 0.1%).

Since film cooling tests were conducted by injecting hot air through the film holes into an ambient mainstream flow, without power being supplied to the surface foils, equation (3) was modified to

$$\eta = \frac{T_f - T_\infty}{T_s - T_\infty} \tag{9}$$

where η is the local film effectiveness, T_f is the local film temperature due to the mixing of hot secondary flow with ambient mainstream flow, T_∞ is the ambient mainstream temperature, and T_s is the secondary flow temperature just before injection.

Since it is very difficult to determine the local film temperature, T_f, an assumption is made. If the test surface was to be adiabatic, there would be no heat transfer at the surface and the local film temperature would have to be equal to the corresponding local adiabatic wall temperature T_{aw}. Therefore, for an adiabatic surface, equation (9) can be modified to

$$\eta = \frac{T_{aw} - T_\infty}{T_s - T_\infty}. \tag{10}$$

Because the test surface was not perfectly adiabatic, q''_{cond} and q''_{rad} had to be accounted for. Since the secondary flow is hotter than the mainstream, there was a conduction gain from within the test model for locations on the leading edge. For locations near the film tubes, there was an additional conduction gain from the hot flow through the injection tubes. This conduction gain resulted in higher wall temperatures on the leading edge. The radiation loss resulted in lower wall temperatures over the entire test surface. These conduction gains and radiation loss were accounted for by dividing their local fluxes by the local heat transfer coefficient to produce an equivalent corrective temperature difference. Thus, equation (10) was modified to

$$\eta = \frac{T_w - T_\infty}{T_s - T_\infty} + \frac{q''_{rad} - q''_{cond}}{h(T_s - T_\infty)} \tag{11}$$

where η is the local film cooling effectiveness, T_w is the local wall temperature without power supply to foils for hot secondary injection into an ambient mainstream, T_∞ is the ambient mainstream temperature, T_s is the hot secondary flow temperature just before injection, q''_{rad} is the local radiation loss flux, q''_{cond} is the local conduction gain flux, and h is the local heat transfer coefficient with film cooling.

For heat transfer tests, since the wall temperature was higher than the ambient mainstream and ambient secondary, equation (4) was modified to

$$\frac{q''}{q''_0} = \frac{h}{h_0}\frac{T_w - T_f}{T_w - T_\infty}. \tag{12}$$

This equation can be used to calculate the local heat load ratio if T_f is determined from η according to equation (9). The equation (12) can be rewritten as

$$\frac{q''}{q''_0} = \frac{h}{h_0}\left(1 - \frac{\eta}{\phi}\right) \tag{13}$$

where η is the local film effectiveness and ϕ is the overall cooling effectiveness given by $\phi = (T_w - T_\infty)/(T_s - T_\infty)$. For gas turbines, the value of ϕ usually ranges from 0.5 to 0.7.

The spanwise averaged heat load ratio was then obtained from

$$\frac{\bar{q}''}{\bar{q}''_0} = \frac{1}{n}\sum_{i=1}^{n}\frac{h(x,z)}{h_0(x,z)}\left(1 - \frac{\eta(x,z)}{\phi}\right) \tag{14}$$

where $\bar{q}''$ is the spanwise averaged convective heat flux with film cooling at any streamwise location x, $\bar{q}''_0$ is the spanwise averaged convective heat flux without film cooling at the same streamwise location, and n is the number of thermocouples in the row at that streamwise location. A typical value of 0.6 was chosen for ϕ.

An uncertainty analysis was carried out for both $Nu_D/(Re_D)^{0.5}$ and η based on the method of Kline and McClintock [16]. Based on 20 : 1 odds, the uncertainty around the film holes was about $\pm 15\%$; whereas, downstream of the film holes, it was about $\pm 5\%$.

RESULTS AND DISCUSSION

The local velocity and turbulence intensity distributions along the centerline and right-side line for both no grid and turbulence grid conditions are shown in Fig. 4. Note that the legend applies to both parts of the figure. The incident mainstream velocity U_∞ at $X/b = 20$ is 10 m s^{-1} for the no grid case. With increasing X/b, due to the approaching stagnation condition, a decrease in the centerline velocity is observed;

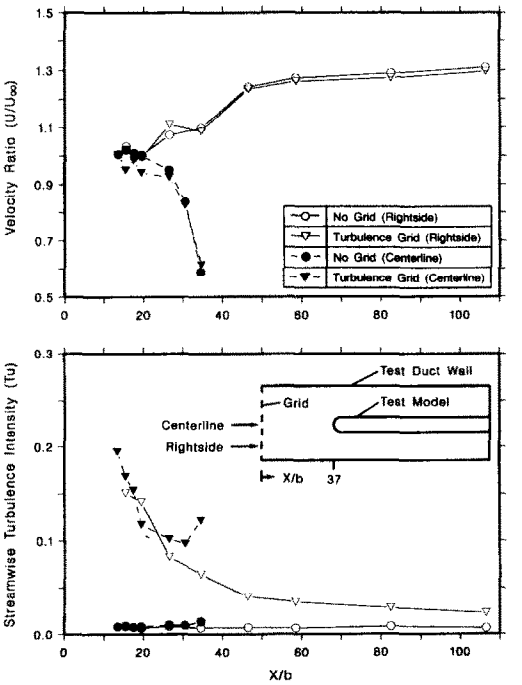

FIG. 4. Streamwise distributions of normalized mainstream velocity and streamwise turbulence intensity.

whereas, due to the blockage effect of the test model, a gradual increase in the right-side line velocity is observed. The turbulence intensity along the right-side line decays with distance as expected. The turbulence intensity along the centerline decays first but as stagnation is approached there is an increase due to a decrease in the local average mainstream velocity. For a given upstream turbulence condition, the minimum value of the corresponding turbulence intensity curve was chosen as the reference turbulence intensity for that condition. Thus, the reference turbulence intensities for the no grid and turbulence grid cases are 0.75 and 9.67%, respectively. Based on the method of Hancock and Bradshaw [17], the corresponding dissipation length scale L_e^u at the same location for the turbulence grid is about 1.5 cm.

The local heat transfer coefficient was non-dimensionalized using $Nu_D = hD/k$, where Nu_D is the local Nusselt number based on the leading edge diameter, h is the local heat transfer coefficient, D is the leading edge diameter, and k is the local fluid thermal conductivity. All local Nu_D values at a given streamwise location were numerically averaged to obtain the spanwise averaged Nusselt number $\overline{Nu}_D$ at that location. Since the flow was laminar, the Reynolds number effect was incorporated by dividing $\overline{Nu}_D$ with $(Re_D)^{0.5}$. All local film effectiveness values at a given streamwise location were numerically averaged to obtain the spanwise averaged film effectiveness $\bar{\eta}$ at that location. The spanwise averaged non-dimensional heat transfer coefficient $\overline{Nu}_D/(Re_D)^{0.5}$ and film effectiveness $\bar{\eta}$ were plotted against the non-dimensional streamwise distance from stagnation x/d.

In Figs. 5–10, the legend in the top part of a figure, if any, applies only to that part; whereas, the legend in the bottom part of a figure applies to both parts of that figure.

The effect of the blowing ratio on the spanwise averaged heat transfer coefficient and film effectiveness for the case of $4d$ injection and no grid case is shown in Fig. 5. Also shown are the low mainstream turbulence no film cooling data from Mick and Mayle [11] and Mehendale *et al.* [15]. From the no film cooling data of Mehendale *et al.*, it is seen that as the distance from stagnation increases, the heat transfer coefficient reduces due to a growing boundary layer until the point of separation. A little downstream of separation, a high heat transfer coefficient is observed due to flow reattachment. These data compare well with the low mainstream turbulence no film data from Mick and Mayle. For the case of secondary injection, peaks are evident just downstream of the film holes at all blowing ratios. This is due to the interaction of the secondary flow with the mainstream. Further downstream of these holes, an increasing boundary layer thickness is seen to cause a reduction in the heat transfer coefficient. An increase in the blowing ratio causes an increased flow interaction, resulting in higher heat transfer coefficients in the leading edge region. Far downstream of the film

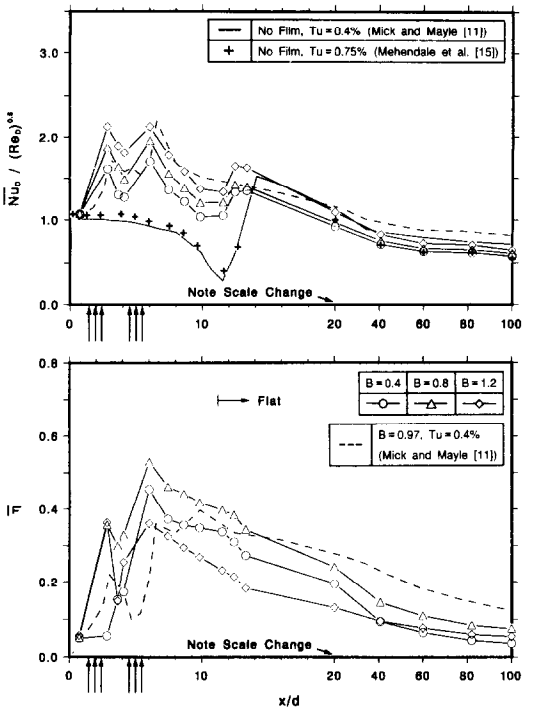

FIG. 5. Effect of the blowing ratio on the spanwise averaged $Nu_D/(Re_D)^{0.5}$ and film effectiveness for the $4d$ spacing injection for the no grid case.

holes, on the flat sidewall, the effect of the blowing ratio is not readily distinguishable. The $B = 0.97$ data from Mick and Mayle [11] are also shown.

The effect of the blowing ratio on the film effectiveness for the no grid case is also shown in Fig. 5.

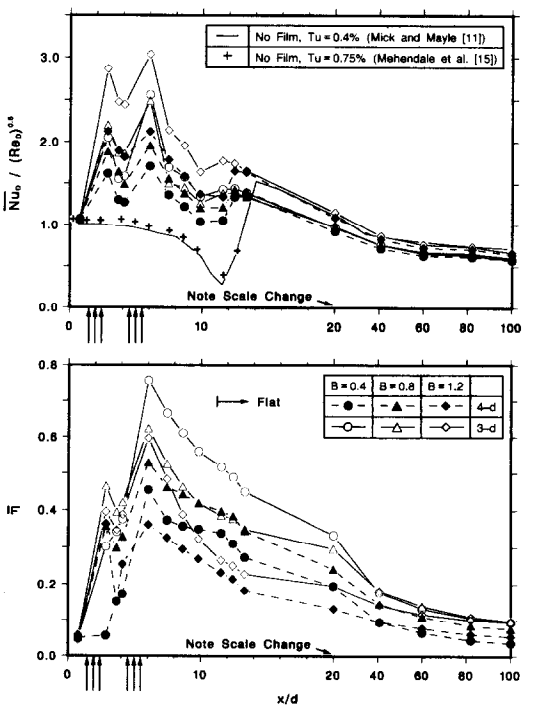

FIG. 6. Effect of the blowing ratio on the spanwise averaged $Nu_D/(Re_D)^{0.5}$ and film effectiveness for the $4d$ and $3d$ spacing injections for the no grid case.

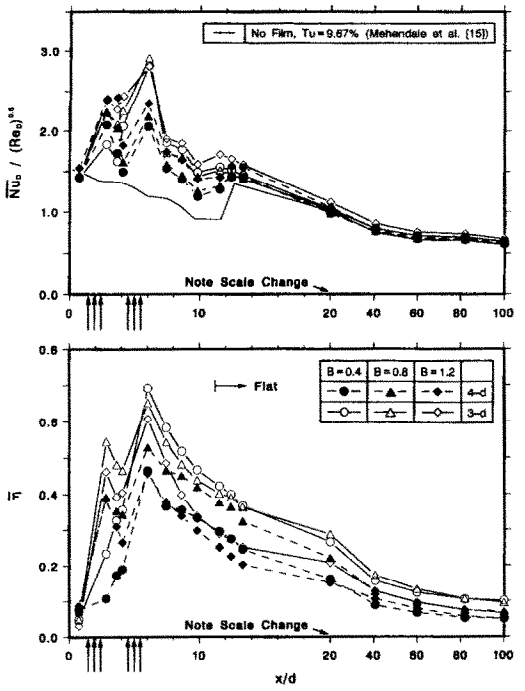

FIG. 7. Effect of the blowing ratio on the spanwise averaged $Nu_D/(Re_D)^{0.5}$ and film effectiveness for the $4d$ and $3d$ spacing injection for the turbulence grid case.

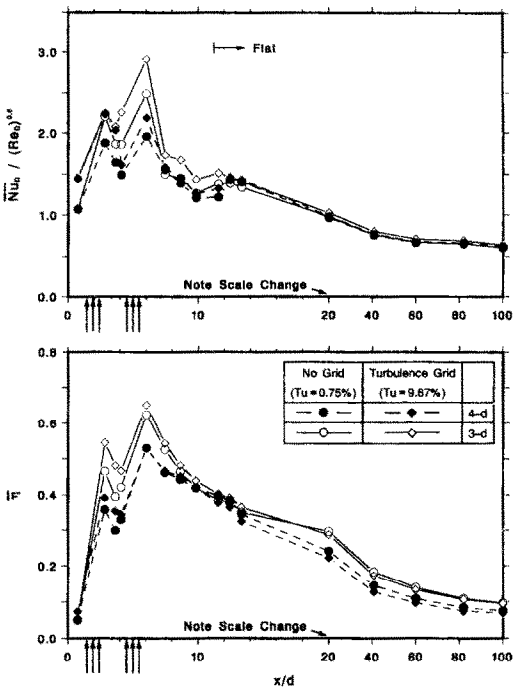

FIG. 9. Effect of the mainstream turbulence on the spanwise averaged $Nu_D/(Re_D)^{0.5}$ and film effectiveness for the $4d$ and $3d$ spacing injections for a blowing ratio of $B = 0.8$.

For the lowest blowing ratio studied of $B = 0.4$, since a very small amount of secondary flow comes out of the film holes at $\pm 15°$, as indicated before in test conditions, the film effectiveness just downstream of the first row of film holes is negligible. Just downstream of the second row of film holes, the film effectiveness reaches a peak value due to more film coverage. Further downstream, the film effectiveness reduces due to dilution of the film. For the highest blowing ratio studied of $B = 1.2$, the secondary jet

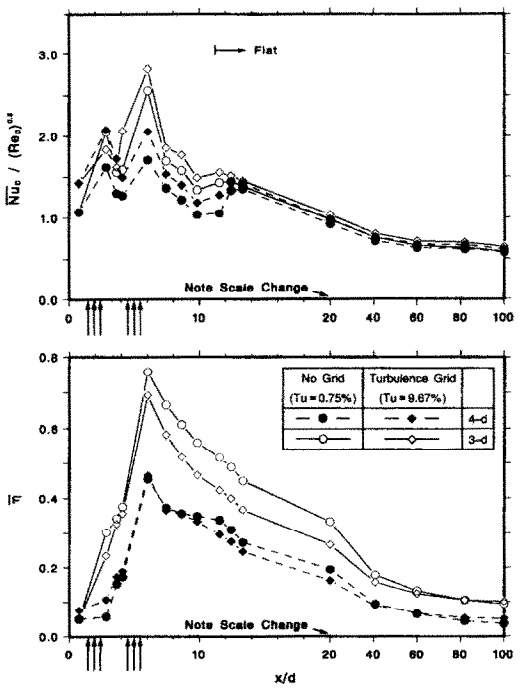

FIG. 8. Effect of the mainstream turbulence on the spanwise averaged $Nu_D/(Re_D)^{0.5}$ and film effectiveness for the $4d$ and $3d$ spacing injections for a blowing ratio of $B = 0.4$.

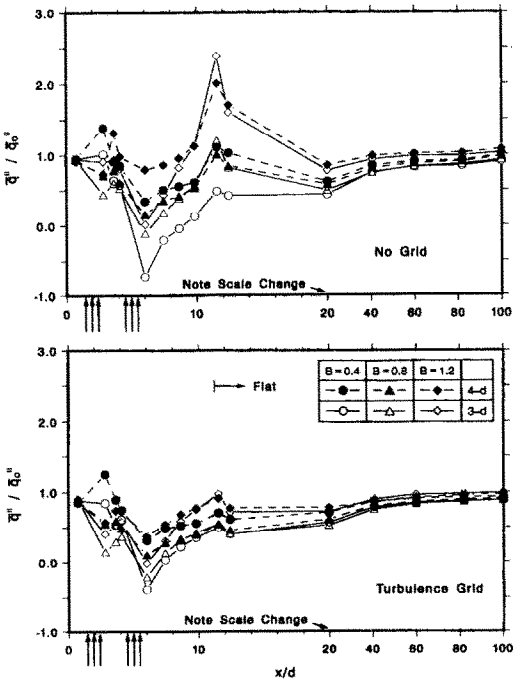

FIG. 10. Effect of the blowing ratio on the spanwise averaged heat load ratio for $4d$ and $3d$ spacing injections for the no grid and turbulence grid cases.

penetrates through the boundary layer thus providing poor film coverage and consequently producing the lowest film effectiveness values. An intermediate blowing ratio of $B = 0.8$ shows the best film effectiveness over most of the test surface. Also shown are $B = 0.97$ film effectiveness data from Mick and Mayle [11].

In Figs. 6–10 and Tables 1 and 2, the results for film holes spaced $3d$ apart are from the results published previously by Mehendale and Han [13].

The effect of the blowing ratio on the spanwise averaged heat transfer coefficient and film effectiveness for the $4d$ and $3d$ injections for the no grid case is shown in Fig. 6. Both injection geometries show that an increase in the blowing ratio causes an increase in the heat transfer coefficient. In the leading edge region, $4d$ geometry shows significantly lower heat transfer coefficients than the $3d$ geometry. This is because, the physical spanwise distance between successive holes is more for $4d$ than for $3d$, thus resulting in lesser flow interaction. For the intermediate blowing ratio of $B = 0.8$, this difference between the two geometries is smallest downstream of the second row of film holes. Due to a physically larger spanwise distance, which results in lesser secondary air coverage, the $4d$ geometry shows a lower film effectiveness than the $3d$ geometry for each blowing ratio. Contrary to the $3d$ case, $B = 0.8$ produces the best film effectiveness for the 4-d case. As for the case of the heat transfer coefficient, downstream of the second row of film holes, the intermediate blowing ratio of $B = 0.8$ produces almost similar values of film effectiveness for the two injection geometries. Film effectiveness for $B = 0.4$ is most adversely affected for the $4d$ case over the $3d$ case. This may be because for $B = 0.4$, the injection jet is too feeble to reach larger spanwise distances in the $4d$ case and may be swept away by the mainstream.

The effect of the blowing ratio on the spanwise averaged heat transfer coefficient and film effectiveness for the turbulence grid case is shown in Fig. 7. As seen in Fig. 6 for the no grid case, the $4d$ injection has lower heat transfer coefficients than the $3d$ injection. As before, an increase in the blowing ratio causes an increase in the heat transfer coefficient for both geometries. For the turbulence grid, this effect of the blowing ratio becomes less prominent for both geometries. This is because, for the lower blowing ratios of $B = 0.4$ and 0.8, the secondary flow turbulence intensities are of the order of 3–5 and 7–12%, respectively (as indicated under 'test conditions'). Therefore, at these lower blowing ratios, the higher mainstream turbulence causes increased mix-

Table 1. Distributions of local $Nu_D/(Re_D)^{0.5}$—$4d$ and $3d$ spacing injections at a blowing ratio of $B = 0.4$ for the no grid and the turbulence grid cases

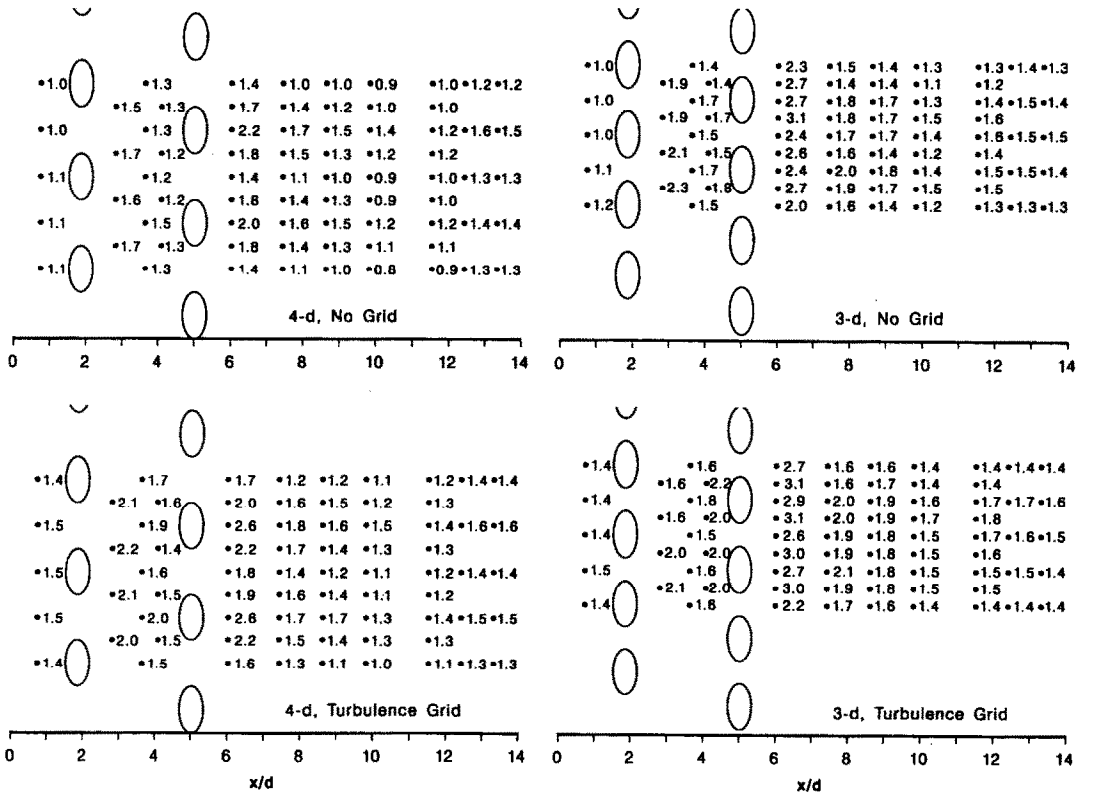

Table 2. Distributions of local film effectiveness—4*d* and 3*d* spacing injections at a blowing ratio of $B = 0.4$ for the no grid and the turbulence grid cases

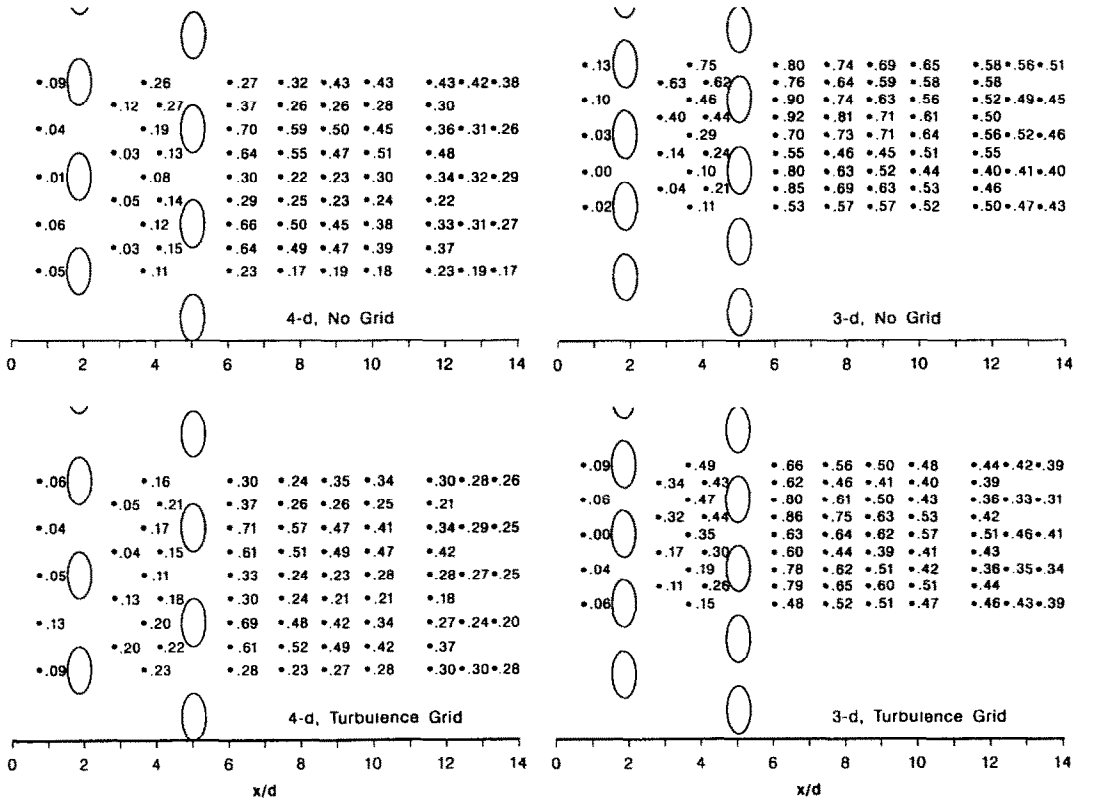

ing between the secondary flow and the mainstream. This results in larger increases in the heat transfer coefficients for the lower blowing ratios, and hence the effect of the blowing ratio on leading edge heat transfer is reduced for the higher mainstream turbulence case. As for the case of low mainstream turbulence in Fig. 6, 4*d* geometry produces lower film effectiveness than the 3*d* geometry due to physically larger spanwise distances. At high mainstream turbulence, as for the case of the heat transfer coefficient, the effect of blowing ratio becomes less prominent for both geometries, since mainstream turbulence dominates as explained above. As in Fig. 6, $B = 0.8$ produces comparable results for both geometries. As compared with the 3*d* case, the film effectiveness at the lowest blowing ratio of $B = 0.4$ is most severely affected for the 4*d* injection.

The effect of the mainstream turbulence on the spanwise averaged heat transfer coefficient and film effectiveness, for the cases of 4*d* and 3*d* injections at the blowing ratio of $B = 0.4$, is shown in Fig. 8. For both geometries, an increase in the mainstream turbulence causes an increase in the heat transfer coefficient on the leading edge. This is because the higher mainstream turbulence penetrates the thin boundary layer on the leading edge, thus producing higher heat transfer coefficients. The heat transfer coefficients for the 4*d* case are lower than for the 3*d* case for both mainstream turbulence cases. This is because of lesser mixing of the flows for the 4*d* case due to physically larger spanwise distances, thus resulting in lower heat transfer coefficients. Increased mainstream turbulence is seen to adversely affect the film effectiveness. This effect of mainstream turbulence is more prominent for the 3*d* case downstream of the second row of film holes. The 3*d* case clearly produces higher film effectiveness than the 4*d* case over the entire test section. This is due to better film coverage on the leading edge for the 3*d* case, whereas, since there is one extra film hole in each row for the 3*d* case over the 4*d* case, more coolant mass comes out for the 3*d* case resulting in a higher film effectiveness on the flat sidewall.

For the intermediate blowing ratio of $B = 0.8$, the effect of the mainstream turbulence on the spanwise averaged heat transfer coefficient and film effectiveness for the cases of the 4*d* and 3*d* geometries is shown in Fig. 9. As in Fig. 8, an increase in mainstream turbulence causes an increase in the heat transfer coefficient. The increases in the heat transfer coefficient, due to the mainstream turbulence, are not as severe as for $B = 0.4$. This may be due to the fact that at $B = 0.8$, the secondary flow turbulence at the exit of the film holes is much higher than that for the

case of $B = 0.4$. For the same reason, the effect of the mainstream turbulence on the film effectiveness becomes less prominent for the higher blowing ratio; and, as before, the $3d$ injection still provides better film coverage.

The effect of the blowing ratio on the spanwise averaged heat load ratio for the case of the $4d$ and $3d$ injections and no grid case is shown in Fig. 10. For the case of the $4d$ injection, the blowing ratio of $B = 0.8$ shows the best performance, whereas, $B = 1.2$ shows the worst performance. This may be due to an optimum film coverage for the intermediate blowing ratio of $B = 0.8$. For the case of the $3d$ injection, an increase in the blowing ratio causes an increase in the heat load ratio. For both these cases, except for the highest blowing ratio of $B = 1.2$, film cooling is seen to reduce the heat load ratio over the entire test surface with $3d$ geometry showing better performance than $4d$ geometry at the corresponding blowing ratios.

The effect of the blowing ratio on the spanwise averaged heat load ratio for the case of the $4d$ and $3d$ injections and the higher mainstream turbulence grid case is also shown in Fig. 10. It is observed that, due to an increase in mainstream turbulence, the effect of secondary flow turbulence is considerably reduced. This is especially so for the highest blowing ratio of $B = 1.2$. It is also observed that at higher mainstream turbulence, film cooling causes a considerable reduction in the heat load ratio at the flow reattachment point for all blowing ratios. Over most of the test surface, the heat load ratios for the turbulence grid case are less than 1.0 unlike for the no grid case. The effect of the blowing ratio on the heat load ratio remains the same as before.

The effect of the mainstream turbulence on the leading edge local heat transfer coefficient, for both cases of the $4d$ and $3d$ injections, for the blowing ratio of $B = 0.4$ is shown in Table 1. In general, the effect of high mainstream turbulence is an increase in heat transfer coefficient at all locations. For the case of the $4d$ injection, variations in both spanwise and streamwise directions are significant; whereas, for the $3d$ injection, variations in streamwise direction are more significant. This is because physically larger spanwise distances for the $4d$ case cause larger spanwise variations as compared with the $3d$ case. As observed before, the $4d$ injection produces lower heat transfer coefficients for both cases of mainstream turbulence.

The effect of the mainstream turbulence on the leading edge local film effectiveness, for both cases of $4d$ and $3d$ injections, for the intermediate blowing ratio of $B = 0.4$ is shown in Table 2. As for the case of the heat transfer coefficients, the $4d$ injection produces significant variations in film effectiveness in both the spanwise and streamwise directions as compared with the $3d$ injection for both cases of mainstream turbulence. In general, an increase in the mainstream turbulence causes a decrease in the film effectiveness; but the film effectiveness for the $4d$ injection is not as severely affected as that for the $3d$ case. The $4d$ injection produces lower film effectiveness for both cases of mainstream turbulence.

CONCLUDING REMARKS

The effect of injection hole geometry on the leading edge heat transfer coefficient and film cooling effectiveness under a high mainstream turbulence condition was experimentally studied for two rows of film holes with film holes spaced four hole diameters and three hole diameters apart. The main findings of the study include:

(1) An increase in the blowing ratio causes an increase in the heat transfer coefficient on the leading edge for all test cases. As the mainstream turbulence increases, there is an increase in the heat transfer coefficient. This effect of the mainstream turbulence reduces for higher blowing ratios.

(2) The $4d$ injection produces lower heat transfer coefficients than the $3d$ injection over the entire leading edge for all three blowing ratios and both cases of mainstream turbulence.

(3) An intermediate blowing ratio of $B = 0.8$ produces the best film effectiveness for the $4d$ geometry; whereas, $B = 0.4$ is the best for the $3d$ geometry for both cases of mainstream turbulence. In general, the leading edge film effectiveness decreases with increasing mainstream turbulence. This effect of mainstream turbulence is seen to reduce at higher blowing ratios.

(4) A higher reduction in the heat load ratio is observed for the high mainstream turbulence case. Blowing ratios of $B = 0.8$ and 0.4 show the best heat load reduction for the $4d$ and $3d$ cases, respectively.

Acknowledgement—The project was sponsored by Textron Lycoming, Inc. through contract No. H164150. Their support is gratefully acknowledged.

REFERENCES

1. R. J. Goldstein, Film cooling. In *Advances in Heat Transfer* (Edited by T. F. Irvine, Jr. and J. P. Hartnett), Vol. 7, pp. 321–379. Academic Press, New York (1971).
2. V. L. Eriksen and R. J. Goldstein, Heat transfer and film cooling following injection through inclined circular tubes, *ASME J. Heat Transfer* **96,** 239–245 (1974).
3. R. E. Mayle, F. C. Kopper, M. F. Blair and D. A. Bailey, Effect of streamline curvature on film cooling, *ASME J. Engng Power* **99,** 77–82 (1977).
4. S. Ito, R. J. Goldstein and E. R. G. Eckert, Film cooling of a gas turbine blade, Tokyo Joint Gas Turbine Cong., Paper No. 03 (1977).
5. J. C. Han and A. B. Mehendale, Flat plate film cooling with steam injection through one row and two rows of inclined holes, *ASME J. Turbomach.* **108,** 137–144 (1986).
6. M. Sasaki, K. Takahara, K. Sakata and T. Kumagai, Study on film cooling of turbine blades, *Bull. JSME* **19**(137), 1344–1352 (1976).
7. D. W. Luckey and M. R. L'Ecuyer, Stagnation region gas film cooling—spanwise angled coolant injection,

TSPC-TR-76-2, Thermal Sciences and Propulsion Center, Purdue University, West Lafayette, Indiana (1976).
8. D. W. Luckey and M. R. L'Ecuyer, Stagnation region gas film cooling—spanwise angled injection from multiple rows of holes, CR-165333, NASA (1981).
9. M. A. Bonnice and M. R. L'Ecuyer, Stagnation region gas film cooling—effects of dimensionless coolant temperature, CR-168197, NASA (1983).
10. J. Karni and R. J. Goldstein, Surface injection effect on mass transfer from a cylinder in crossflow: a simulation of film cooling in the leading edge region of a turbine blade, ASME Paper No. 89-GT-276 (1989).
11. W. J. Mick and R. E. Mayle, Stagnation film cooling and heat transfer, including its effect within the hole pattern, *ASME J. Turbomach.* **110**, 66–72 (1988).
12. V. Nirmalan and L. O. Hylton, An experimental study of turbine vane heat transfer with leading edge and downstream film cooling, ASME Paper No. 89-GT-69 (1989).
13. A. B. Mehendale and J. C. Han, Influence of high mainstream turbulence on leading edge film cooling heat transfer, *ASME J. Turbomach.* (in press).
14. S. Ou, A. B. Mehendale and J. C. Han, Influence of high mainstream turbulence on leading edge film cooling heat transfer: effect of film hole row location, *ASME J. Turbomach.* (in press).
15. A. B. Mehendale, J. C. Han and S. Ou, Influence of high mainstream turbulence on leading edge heat transfer, *ASME J. Heat Transfer* **113**, 843–850 (1991).
16. S. J. Kline and F. A. McClintock, Describing uncertainties in single-sample experiments, *Mech. Engng* **75**, 3–8 (1953).
17. P. E. Hancock and P. Bradshaw, The effect of free-stream turbulence on turbulent boundary layers, *ASME J. Fluids Engng* **105**, 284–289 (1983).

INFLUENCE D'UNE TURBULENCE ELEVEE SUR LE TRANSFERT THERMIQUE DE REFROIDISSEMENT PAR FILM AU BORD D'ATTAQUE: EFFET DE L'ESPACEMENT DES TROUS

Résumé—L'effet de la géométrie du trou d'injection sur le coefficient de transfert thermique au bord d'attaque et sur l'efficacité du refroidissement par film, sous la condition de forte turbulence principale, est étudié expérimentalement pour un nombre de Reynolds de 100000. Des données sont obtenues pour trois rapports de soufflage de 0,4, 0,8 et 1,2 à travers deux rangées de trous logées à $\pm 15°$ et $\pm 40°$ pour deux géométries d'injection: (a) trous espacés de quatre diamètres et (b) trous espacés de trois diamètres dans la direction de l'envergure. Les résultats montrent que le coefficient de transfert thermique au bord d'attaque augmente et que l'efficacité du film diminue quand la turbulence principale augmente; néanmoins, l'effet diminue lorsque le rapport de soufflage augmente. Le transfert thermique au bord d'attaque avec injection de réfrigérant pour le cas des trois diamètres est inférieur à celui du cas à quatre diamètres pour une faible turbulence principale, mais la différence diminue pour une turbulence plus forte.

EINFLUSS EINER HOHEN HAUPTSTROMTURBULENZ AUF DEN WÄRMEÜBERGANG DURCH FILMKÜHLUNG AN DER ANSTRÖMKANTE: EFFEKT DES BOHRUNGSABSTANDES

Zusammenfassung—Der Einfluß der Geometrie der Einströmbohrungen auf den Wärmeübergangskoeffizienten an der Anströmkante und die Wirksamkeit der Filmkühlung wird unter den Bedingungen einer starken Hauptstromturbulenz für Reynolds-Zahlen um 100000 experimentell untersucht. Es werden Versuchsdaten für drei Einblasverhältnisse (0,4; 0,8; 1,2) durch zwei Reihen von Bohrungen (angeordnet bei $\pm 15°$ und $\pm 40°$) für zwei Einblasgeometrien ermittelt: (a) Querteilungsverhältnis 4 und (b) Querteilungsverhältnis 3. Die Ergebnisse zeigen, daß der Wärmeübergangskoeffizient an der Anströmkante mit wachsender Turbulenz der Hauptströmung zunimmt, während die Effektivität der Filmkühlung abnimmt. Dieser Effekt nimmt jedoch mit zunehmendem Einblasverhältnis ab. Bei geringer Turbulenz der Hauptströmung ist der Wärmeübergang an der Anströmkante mit Einblaskühlung im Fall der Querteilung drei geringer als bei der Querteilung vier. Bei höherer Turbulenz der Hauptströmung nimmt der Unterschied ab.

ВЛИЯНИЕ ИНТЕНСИВНОЙ ТУРБУЛЕНТНОСТИ ОСНОВНОГО ПОТОКА НА ТЕПЛОПЕРЕНОС У ПЕРЕДНЕЙ КРОМКИ ПРИ ПЛЕНОЧНОМ ОХЛАЖДЕНИИ

Аннотация—Экспериментально исследуется влияние геометрии отверстий для вдува на коэффициент теплопереноса у передней кромки и эффективность пленочного охлаждения в условиях интенсивной турбулентности основного потока при числе Рейнольдса, равном 100000. Получены данные для трех значений параметра вдува, составляющих 0,4; 0,8 и 1,2, через два ряда отверстий, расположенных под углами ± 15 и $\pm 40°$, для двух геометрий вдува, когда расстояние между отверстиями в направлении течения равно четырем и трем диаметрам отверстий соответственно. Результаты показывают, что коэффициент теплопереноса у передней кромки увеличивается, а эффективность пленочного охлаждения уменьшается по мере возрастания турбулентности основного потока, однако этот эффект уменьшается с ростом параметра вдува. При малой интенсивности турбулентности в случае расстояния, равного трем диаметрам отверстий, теплоперенос у передней кромки при вдуве тяплоносителя (тепловой нагрузке) меньше, чем в случае расстояния, равного четырем диаметрам, но в условиях более интенсивной турбулентности это различие уменьшается.